DOI: 10.1002/chem.200903403

Dynamic Vapochromic Behaviors of Organic Crystals Based on the Open–Close Motions of S-Shaped Donor–Acceptor Folding Units

Eiji Takahashi,[a] Hikaru Takaya,*[a, b] and Takeshi Naota*[a]

Abstract: The first vapochromic organic crystals are described with respect to their preparation, color change, adsorption/desorption properties, crystal structures, and color-change mechanism. Non-solvatochromic, 1,4,5,8-naphthalene-tetracarboxylic diimide (NDI) derivatives **1a** bearing two pyrrole imine (PI) tethers have been used as a motif for the crystal packing template. Red-purple vapochromic solid **3** was prepared by evacuation of orange crystals **2** (equivalent to **1a**·2 MeOH), obtained by recrystallization of **1a** from MeOH. Solid **3** showed high-adsorption ability and unprecedented vapor-dependent color changes upon exposure to a variety of organic vapors, whereas light brown amorphous solid **1a**, did not show vapo- or solvatochromic behavior toward any organic solvent. The strong adsorption capability of **3** was confirmed by TGA experiments and adsorption/desorption isotherms. Analysis of the solid-state UV/Vis analysis revealed that the vapor-dependent color changes of **3** were owed to the specific interference of solvent vapors with its broad CT absorbance at $\lambda = 450$–650 nm. Packing structures of **1a** in orange crystals **2**, red-purple solid **3**, and regenerated orange solid **2** were unequivocally established by single crystal and synchrotron powder X-ray diffraction, respectively. Molecular structures and arrays of **1a** in these materials indicated that 1) unit **1a** had an S-shaped folded conformation in **2** and **3** by intramolecular donor–acceptor interactions between NDI and two PI units; 2) inclusion of the guest vapor into the S-shaped template decreased the intramolecular PI-NDI interactions, accompanied by increasing intermolecular NDI-NDI and PI-PI interactions; and 3) such flexible, open–close motions of the S-shaped template could be repeated during reversible adsorption/desorption processes without degradation of crystal packing. The adsorption properties and mechanism of molecular shape-dependent vapochromic behavior of **3** are discussed with reference to experimental results, crystallographic data, and theoretical calculations.

Keywords: host–guest systems · pyrroles · sensors · vapochromism · X-ray diffraction

Introduction

Development of vapochromic materials and their mechanistic studies are subjects of importance in view of basic science of stimuli-responsive color change,[1–8] and future applications in sensing volatile organic compounds.[9] Two major strategies have been adopted to bestow vapochromic properties on materials. One is the immobilization of solvatochromic π-conjugated organic dyes in insoluble polymeric materials, such as sugar gel,[1] mesoporous silica,[2] or poly(vinylpyrrolidone),[3] in which slight color changes occur upon exposure to organic vapors, by regional aggregation of substituted dye moieties on the "wet" solid surfaces of polymer chains. An alternative strategy is to design porous crystals of organometallic compounds. Remarkable changes in color and emission have been observed using a variety of transition-metal assemblies for which adsorption and desorption of organic vapors lead to significant variations in M–M interactions,[4,5] coordination modes,[6] conformation of π-conjugated ligands[7] and stacking interactions between coordination planes.[8] Crystal design is a forward-looking strategy for the development of functional vapochromic materials, as adsorption properties and color change can be

[a] E. Takahashi, Dr. H. Takaya, Prof. Dr. T. Naota
Department of Chemistry
Graduate School of Engineering Science
Osaka University
Machikaneyama, Toyonaka, Osaka 560-8531 (Japan)
Fax: (+81) 6-6850-6222
E-mail: naota@chem.es.osaka-u.ac.jp
takaya@chem.es.osaka-u.ac.jp

[b] Dr. H. Takaya
PREST (Japan) Science and Technology Agency (JST)
Machikaneyama, Toyonaka, Osaka 560-8531 (Japan)

Supporting information for this article is available on the WWW under http://dx.doi.org/10.1002/chem.200903403.

controlled by rational design of molecular crystals without reliance on the solvatochromic behavior of the molecules.

The creation of vapochromic organic crystals without a transition metal core is a matter of great urgency, owing to the low cost and a variety of molecular designs. Nevertheless, there have been no studies on the vapochromism of organic crystals, probably owing to their imagined low adsorption ability in comparison to metal–organic framework systems,[4k,6a,7] and the absence of d orbital interactions needed for versatile color change. As part of our program aimed at the creation of new organic functional materials, we have been investigating the development of functional organic crystals utilizing 1,4,5,8-naphthalenetetracarboxylic diimide (NDI), which provides molecules with specific assembling,[10,11] folding[12,13] and chromic[11] behaviors, owing to its planar structure and strong π-electron accepting properties.[14] In this paper, we describe the first vapochromic organic crystals in which flexible open–close motions of S-shaped, donor-linked NDI unit results in strong adsorption properties and molecular shape-dependent color changes upon exposure to a variety of organic vapors.

An outline of the mechanism of color change upon adsorption and desorption of organic vapors is shown in Scheme 1. We used compound **1a** (PINDI) as a unit of vapochromic organic crystal. In this compound, the potentially chromic NDI[11,13] moiety was doubly connected to pyrrole imine (PI) units through trimethylene spacers. This compound readily gave orange crystals **2** from MeOH solution, in which each unit of **1a** had an S-shaped, folded conformation[12,13] by intramolecular donor–acceptor interactions between NDI and PI units. Two MeOH molecules were included tightly in the cavity of this S-shaped template with strong H-bonding to nitrogen atoms of the pyrrole and imine moieties. Evacuation of **2** afforded a thermally stable, red-purple solid **3**, in which the intramolecular stacking of each **1a** unit was enhanced without degradation in crystal packing. Guest-free, porous solid **3** strongly adsorbed a variety of organic vapors. Capture of planar aromatic, or H-bonding small guest molecules weakened the PI-NDI stacking, whereas large H-bonding guest molecules mainly interfered sterically with this interaction. Such flexibility in the D–A interactions of the S-shaped template gave rise to its unprecedented molecular-shape dependent vapochromism. It should be noted that these chromic behaviors could be observed exclusively when these precisely engineered crystals were employed. The light-brown amorphous solid **1a**, did not display vapochromism, nor did its pale-orange solution display any solvatochromism. This article investigates in detail this new class of vapochromic organic crystals, including their preparation, color change, adsorption/desorption properties, crystal structure, and color-change mechanism.

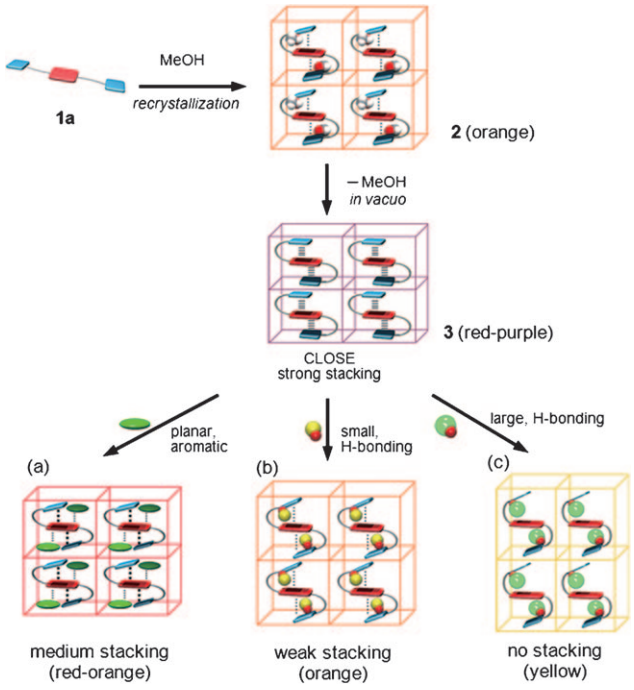

Scheme 1. Schematic representation for the open–close motions of **1a** in vapochromism of PINDI crystals.

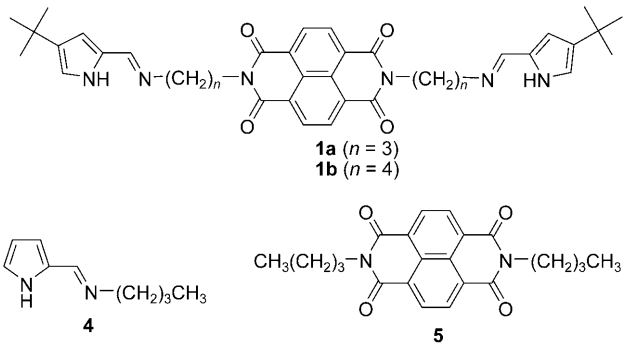

Results and Discussion

Preparation and vapochromic behavior of PINDI crystals: PINDI **1a** was prepared quantitatively by the condensation of *N*,*N*′-bis(3-aminopropyl)-1,4,5,8-naphthalenetetracarboxylic diimide[15] with 4-*tert*-butylpyrrole-2-carboxaldehyde.[16] Orange needles of the template compound **2** (**1a**·2MeOH) were readily obtained upon recrystallization of **1a** from MeOH. Other organic solvents failed to yield crystals of their respective inclusion complexes in satisfactory quality and quantity. Trial recrystallizations of PINDI analogues such as **1b** ($n=4$) and various perylene diimide (PDI) derivatives also gave unsatisfactory results. Orange needles of **2** thus obtained can be converted into brilliant red-purple needles **3** upon removal of MeOH under reduced pressure at 353 K. Crystals **3** were thermally stable and reasonably impervious to air. Optical microscope images of needles **2** and **3** are shown in Figure 1.

Exposure of red-purple **3** to various organic vapors caused significant changes in color, to orange-red (benzene, toluene, hexane), orange (MeOH, EtOH, *n*PrOH, acetone,

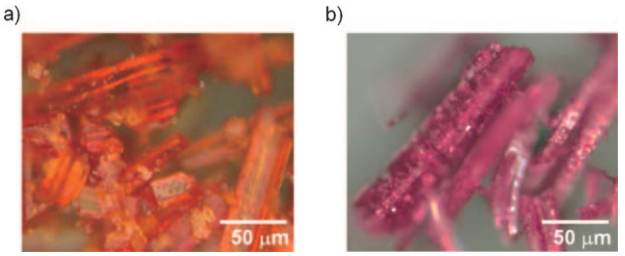

Figure 1. Optical microscope images of a) orange needles **2** (PINDI·2 MeOH) and b) red-purple needles **3** (PINDI).

THF, DMSO), or yellow (*i*PrOH, 2-butanol, *t*BuOH, Et_3N, HCHO). Photos of typical color changes of **3** are shown in Figure 2. The orange solids containing adsorbed MeOH,

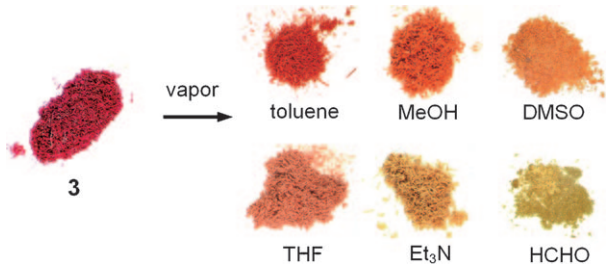

Figure 2. Color changes of **3** after exposure to saturated vapors of various volatile organic compounds.

EtOH, or *n*PrOH vapors could be converted to the original red-purple **3**, upon evacuation. This color change between red-purple and orange could be repeated indefinitely at room temperature with no measurable crystal degradation. Color changes of **3** with other VOCs were irreversible. The distinct color change observed with HCHO vapor (red-purple to yellow) would be important in view of its potential applicability to the future monitoring systems for sick house syndrome gases.[9] It was noteworthy that the color seen with primary alcohols (orange) was different from that observed for secondary and tertiary alcohols (yellow). This was therefore a rare case of vapochromism for which the color change depended significantly on the shape of the vapor molecules. This vapochromism was observed exclusively when porous solid **3** or its ground powder was used as the adsorbent. Light-brown amorphous solid **1a**, prepared by vacuum freeze-drying of a solution of **1a** in benzene, did not adsorb or display vapochromic behavior towards any organic vapor. In addition, all solutions of **1a** in organic solvents were pale orange irrespective of temperature, concentration, or solvent type. Other related materials, such as PINDI analogue **1b**, a 1:1 mixture of butyl(pyrrol-2-yl-methylene)amine **4** and *N*,*N*′-dibutyl-1,4,5,8-naphthalenetetracarboxylic diimide **5**, and various other PDI derivatives did not show vapo- or solvatochromic behaviors in any organic vapor or solvent, respectively.

Response times for color change of **3** were investigated with various organic vapors. When finely ground crystals **3** were exposed to saturated organic vapors at room temperature, the color changes were finished approximately in the following order: MeOH, acetone, THF (within 1 min) > Et_3N, benzene (within 5 min) > EtOH, *n*PrOH, toluene (within 10 min) > *i*PrOH, 2-butanol, *t*BuOH, hexane (within 20 min) > HCHO(2 days) > DMSO (3 days). Response for HCHO vapor is reasonably slow in this test, as 30% aqueous solution (formalin) was used for the source of organic vapor. Owing to the strong adsorption capability of **3**, these color changes could be accelerated considerably at higher temperatures. Typically, the color change of **3** with saturated DMSO vapor (yellow) was complete within 30 min at 60°C. The above vapochromic behaviors can be also observed when low concentrations of MeOH (1.7×10^3 ppm) toluene (2.1×10^3 ppm), THF (2.8×10^3 ppm), and triethylamine (1.6×10^3 ppm) vapors were exposed to the finely ground **3** at room temperature, although prolonged exposure times of several hours were required for sufficient color changes.

Morphology of crystals strongly affects rate of the color change. First, three different sizes of crystals **2** were prepared by three methods: a) recrystallization of **1a** from MeOH, b) the recrystallization and subsequent grinding of the resulting needles **2** with spatula, and c) the recrystallization and subsequent sonication in MeOH. Three red-purple samples, **3**, were prepared by evacuation of each orange solid, **2**. Figure 3 shows SEM images of different morphologies of solid **3** in which approximate sizes of crystals are in the range of a) 100–1000 μm, b) 20–100 μm, and c) 10–50 μm, respectively. Long needles **3** (method a, Figures 1b and 3a) require over 2 min for completion of color change upon exposure to saturated MeOH vapor at room temperature, whereas microcrystals prepared by manual glinding (method b, Figures 2 and 3b) completes the color change after 1 min. The sample prepared upon sonication (method c, Figure 3c) acts as the most efficient adsorbent, and the response time is within 1 min. Although the adsorption rate (red-purple **3** to orange **2**) clearly depends on the size of crystals, desorption rate (**2** to **3**) is not affected by the mor-

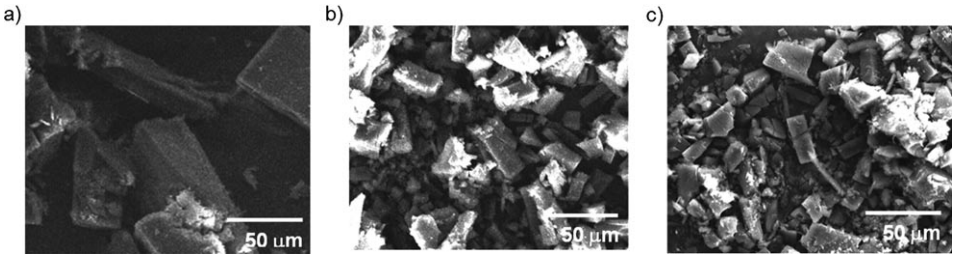

Figure 3. SEM images of red-purple solids **3**, prepared by a) recrystallization of **1a** from MeOH and evacuation, b) the recrystallization, manual grinding, and evacuation, and c) the recrystallization, sonication (0.45 W cm^{-2}, 40 KHz, 1 min) in MeOH, and evacuation.

phology of the crystals. Upon standing under air at room temperature, all three orange samples **2** required 2 h for sufficient color change to red-purple.

Solid-state UV/Vis spectra of **3** before and after exposure to representative VOCs are shown in Figure 4 and Figure 5. Powder **3** had an extraordinarily intense, broad absorption band at $\lambda = 450$–650 nm, attributable to charge-transfer (CT) from PI to NDI caused by their intramolecular stacking.[13a–c,e]

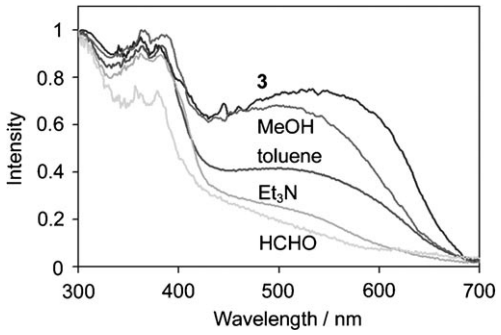

Figure 4. Solid state UV/Vis spectra of **3** after exposure to typical organic vapors.

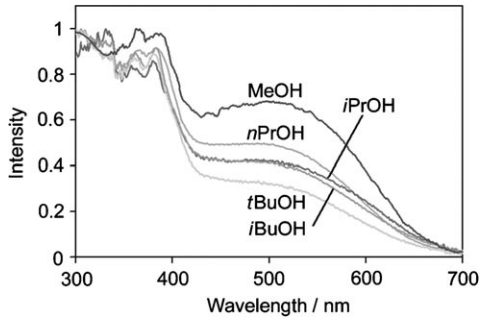

Figure 5. Changes in solid state UV/Vis spectra of **3** after exposure to various alcohol vapors.

Amorphous solid **1a** did not have a significant CT absorbance either in the solid state or in solution in any organic solvent (Figure 6). Absorption spectra of solutions of **1a** showed no significant dependence on temperature, concentration, or solvent type, showing that **1a** possessed negligible solvatochromic and aggregation behavior in solution. Adsorption of MeOH, DMSO, Et_3N, or HCHO vapors by **3** decreased the intensity of this broad CT band significantly in the order: MeOH < DMSO < Et_3N < HCHO, which explained the color changes from red-purple to orange (MeOH, DMSO) and yellow (Et_3N, HCHO). In particular, the adsorption of HCHO strongly quenched this CT interaction. Adsorption of toluene gave rise to a rather different CT band, characteristically enriched at $\lambda = 550$–650 nm. This was the reason for the red-orange color of this substance, although the intensity of its CT band was much weaker than that of MeOH. The UV/Vis spectra of **3** upon adsorption of various alcohols are depicted in Figure 5. Different alcohols quenched the CT absorbance of **3** to different degrees, in the order: primary < secondary < tertiary, which meant that the steric bulk of the guest alcohols is a major factor in controlling the color change.

Adsorption/desorption properties: Exposure of **3** to MeOH, EtOH, *i*PrOH, THF, and toluene vapors caused an increase in sample weight, corresponding to inclusion of 2.0, 2.0, 1.4, 1.7, and 1.5 equivalents of the guest molecules, respectively. The estimated equivalents of adsorbed HCHO were a surprisingly high 6.3, much higher than for the other molecules adsorbed. Adsorption/desorption properties of PINDI were investigated by studying the reversible color change between orange **2** and red-purple **3**. Gravimetric measurements and elemental analyses indicated that crystalline **2**, solid **3**, and regenerated solid **2** (recycled) were equivalent to **1a**·2MeOH, **1a**, and **1a**·2MeOH, respectively. Thermogravimetric analysis of crystals **2** from 30°C to 180°C indicated that crystals **2** suddenly decreased in weight at 100–110°C (Figure 7). The total weight loss of 8.8% accorded well with the theoretical value (9.0%) calculated for the dissociation of two MeOH molecules. Figure 8 shows the adsorption/desorption isotherms of **3** at 298 K. The adsorption profile clearly consisted of a two-step process in which one equivalent of MeOH was adsorbed strongly until $P/P_0 = 0.03$, after which the subsequent hysteretic adsorption of a second equivalent appeared at $P/P_0 = 0.17$. On the contrary, no significant desorption profile was observed until the pressure

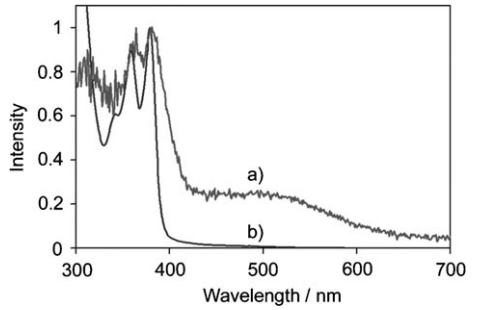

Figure 6. UV/Vis spectra of a) amorphous solid **1a** prepared by vacuum freeze-drying and b) a 0.02 mM solution of **1a** in MeOH.

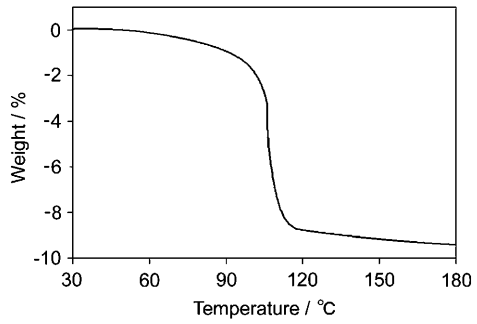

Figure 7. Thermogravimetric trace showing the weight loss in crystals of **2**.

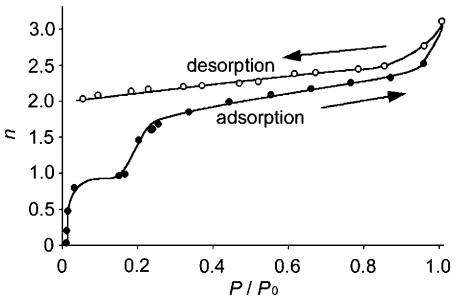

Figure 8. Methanol adsorption (●)/desorption (○) isotherms of powder **3** at 298 K, for which n was calculated as the number of moles of adsorbed MeOH per mole of **1a**. P_0 is the saturated vapor pressure of MeOH (16.917 kPa).

decreased to $P/P_0 = 0.055$. These results plainly indicated that 1) the color change of **3** from purple to orange occurred by the stepwise adsorption of two equivalents of MeOH, and 2) porous solid **3** had high guest-binding capability even at relatively high temperatures.

Molecular structure of PINDI crystals: Alterations in the structure of **1a** upon conversion to **2** and **3**, occurring during desorption/adsorption of MeOH vapor, were confirmed by X-ray crystallography. The molecular arrangement of **1a** in crystalline **2** (**1a**·2MeOH) were determined by single-crystal X-ray diffraction of orange needles obtained by recrystallization of **1a** from MeOH. Analytical grade **3** was obtained by evacuating crystals of **2** and subsequently recrystallizing the resulting crude **3** from toluene. Although this process resulted in the contamination of the sample by a considerable amount of orange-red crystals of the toluene complex, pure red-purple **3** could be separated manually from the mixture because of its distinct color. Analytical grade, regenerated orange powder **2** (recycled) was obtained by exposure of crude red-purple solid **3** to MeOH vapor. Samples of **3** and **2** (recycled) were analyzed by synchrotron-radiation powder-diffraction experiments at SPring-8, Japan, and their crystal structures were refined with the DASH[17] and RIETAN-FP[18] programs. Crystallographic data for as-prepared **2**, and recycled **3** and **2** are listed in Table 1. The XRD pattern of crude **3** obtained from simple evacuation of orange crystals **2** matched that of the analytical grade sample of **3** (see the Supporting Information), indicating that these two crystal structures were identical.

An ORTEP drawing of **1a**·2MeOH in crystals of **2** is shown in Figure 9. The distinct S-shaped folded conformation arose from double-sided association of the NDI unit[12,13] with two PI termini. The average distance between NDI and PI planes was 3.322 Å. Each MeOH guest molecule was included in one of two symmetric cavities of the S-shaped template with strong assistance from two different hydrogen bonds: active hydrogen of MeO*H* with imine nitrogen *N*(2), and oxygen of Me*O*H with active hydrogen of pyrrole N(3)*H*. Molecular structures of **1a** in **3** and **2** (recycled) are shown in Figure 10. All bond lengths of **1a** in **3** and **2** (recycled) coincided with those in crystalline **2** within 1% deviation (see the Supporting Information). This was a good indication that the present analytical method using synchrotron radiation was highly reliable. The conformation of **1a** in powder **3** remained S-shaped (Figure 10a), but the average PI-NDI distance (3.292 Å) was significantly shorter than in crystals of **2** (3.322 Å) owing to the absence of the MeOH guests in **3**. The molecular structure and all bond parameters of **1a** in powder **2** (recycled) were almost the same as those of crystalline **2**, as shown in Figure 9 and Figure 10b and in the Supporting Information. These results indicated that no measurable disorder of crystal packing took place, at least during a batch regeneration process including removal of MeOH from orange crystals **2** in vacuo, grinding of resulting red-purple **3** into a micropowder, and subsequent adsorption of MeOH vapor.

Table 1. Crystallographic data and Rietveld refinement summary.

Solid number	**2**	**3**	**2** (recycled)
compound	**1a**·2MeOH	**1a**	**1a**·2MeOH
form	orange needles	red-purple powder	orange powder
preparation	recrystallization of **1a** from MeOH	removal of MeOH from **2** in vacuo, and subsequent recrystallization from toluene	exposure of **3** to MeOH vapor
empirical formula	$C_{40}H_{50}O_6N_6$	$C_{38}H_{42}O_4N_6$	$C_{40}H_{50}O_6N_6$
crystal system	triclinic	triclinic	triclinic
space group	$P\bar{1}$ (no. 2)	$P\bar{1}$ (no. 2)	$P\bar{1}$ (no. 2)
a [Å]	7.286(1)	14.349(1)	7.265(1)
b [Å]	11.413(2)	9.104(2)	11.436(1)
c [Å]	11.878(3)	7.199(1)	11.863(1)
α [°]	75.336(6)	82.844(6)	75.358(5)
β [°]	78.000(8)	106.176(7)	78.092(4)
γ [°]	81.723(8)	92.454(7)	81.679 (4)
V [Å^3]	930.4(3)	896.1(18)	928.6(11)
Z	1	1	1
T [K]	111	300	100
radiation used (λ [Å])	$Mo_{K\alpha}$ (0.71075)	synchrotron (1.30)	synchrotron (1.30)
2θ [°]	54.9[a]	3.01–60	2.01–58
R[b]	0.052	–	–
R_w[c]	0.159	–	–
R_p	–	8.45	4.80
R_{wp}	–	11.80	7.08
S	–	2.2581	2.7284
G.o.F.	1.01	–	–

[a] Maximum value. [b] $R = \Sigma(F_o^2 - F_c^2)/\Sigma F_o^2$. [c] $R_w = \{\Sigma\omega(F_o^2 - F_c^2)^2/\Sigma\omega(F_o^2)^2\}^{1/2}$.

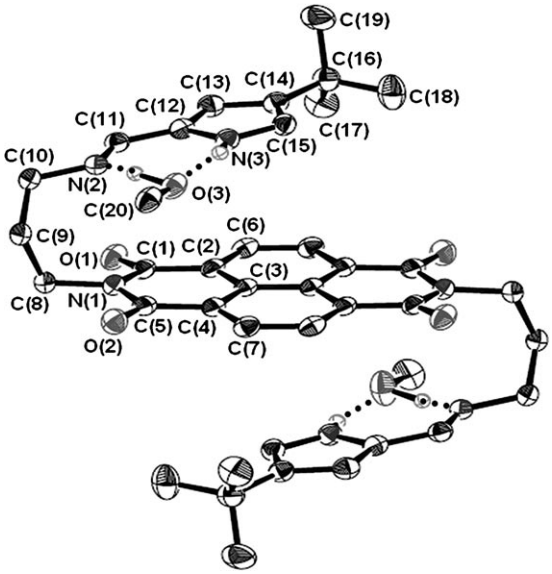

Figure 9. ORTEP representation of **1a**·2MeOH in orange crystals **2** at the 50% probability level. Selected bond lengths [Å] and angles [°]: C(1)–C(2) 1.480(3), C(2)–C(3) 1.414(3), C(2)–C(6) 1.379(2), C(1)–O(1) 1.214(3), C(1)–N(1) 1.395(2), C(8)–N(1) 1.480(2), C(10)–N(2) 1.464(2), C(11)–N(2) 1.281(2), C(12)–C(13) 1.387(3), C(12)–N(3) 1.367(3), C(13)–C(14) 1.417(3), C(14)–C(15) 1.378(3), C(15)–N(3) 1.366(2), C(20)–O(3) 1.418(3); O(1)-C(1)-N(1) 121.3(2), N(2)-C(11)-C(12) 123.0(2), C(12)-N(3)-C(15) 109.3(2).

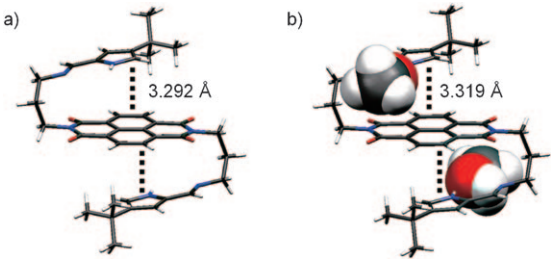

Figure 10. Molecular structures and intramolecular stacking interactions of **1a** in a) red-purple powder **3** and b) orange powder **2** (recycled).

The intermolecular stacking pattern in powder **3** was also different from that in crystalline **2** and powder **2** (recycled). Figure 11 shows the crystal packing of **1a** in powder **3** and recycled powder **2**. In the latter, each molecular unit of **1a** in its arrays participated in intermolecular PI-PI and NDI-NDI interactions with stacking distances of 3.194 and 3.307 Å, respectively (Figure 11b). These values were almost the same as those obtained from single-crystal X-ray diffraction patterns of crystalline **2** (PI-PI, 3.192 Å; NDI-NDI, 3.304 Å). In contrast, molecular units **1a** in powder **3** had no significant PI-PI interactions, and the intermolecular stacking distance between NDI-NDI planes was much longer (3.445 Å) than in **2** (Figure 11a). Thus, inclusion of MeOH guests enhanced the PI-PI and NDI-NDI interactions, but diminished the PI-NDI interactions. In other words, intra- and intermolecular interactions were alternately turned on or off, respectively, upon inclusion or dissociation of MeOH guests during the reversible color change between orange and red-purple.

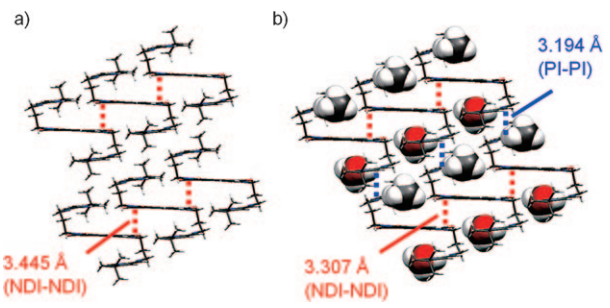

Figure 11. Crystal packing and intermolecular stacking interactions of **1a** in a) red-purple powder **3** and b) orange powder **2** (recycled).

The reversibility of the structural transition between **2** and **3** was indicated by several XRD spectra taken during repeated desorption/adsorption processes, as shown in Figure 12. The XRD spectrum of powder **3** obtained from crystalline **2** was exactly the same as that of recycled powder **3**, produced by the adsorption and subsequent de-

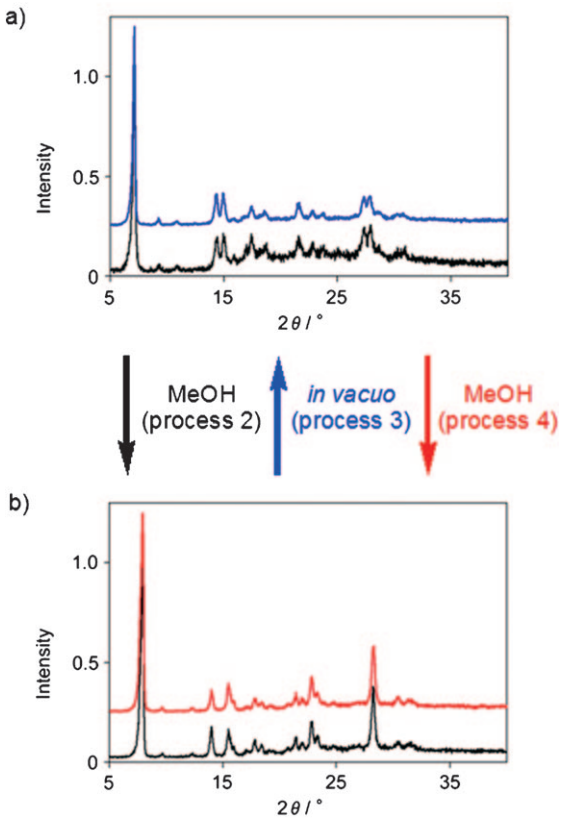

Figure 12. X-ray powder diffraction patterns of a) **3** and b) **2** at room temperature after consecutive recycling processes. Black line in a): red-purple powder **3** after removal of MeOH from fresh crystals of orange **2** in vacuo (process 1). Black line in b): orange powder **2** after exposure of red-purple powder **3** to MeOH vapor (process 2). Blue line in a): red-purple powder **3** after removal of MeOH from orange powder **2** in vacuo (process 3). Red line in b): orange powder **2** after exposure of red-purple powder **3** to MeOH vapor (process 4).

sorption of MeOH (Figure 12a, processes 1–3). In addition, the XRD pattern of powder **2** after the first recycling remained the same after a second recycling process (Figure 12b, processes 2–4). Adsorption and desorption processes did not generate any disorder in the crystal packing of PINDI, owing to the aforementioned intra- and intermolecular stabilizations. The structural changes in PINDI crystals were investigated precisely during the thermal transformation of **2** to **3** by a temperature-dependent XRD analysis, which proved illuminating. Figure 13 shows X-ray diffractograms of crystals **2** in the temperature range 300–430 K. The sharp and intense signal of **2** at $2\theta = 6.8°$ decayed with increasing temperature, and finally disappeared at 360 K. The signal of **3** at $2\theta = 3.0°$ began to be observed from 350 K, and its intensity increased at higher temperatures. During the transformation of **2** to **3**, an unidentified pattern bearing a sharp signal at $2\theta = 6.0°$ appeared at 320 K, reached maximum intensity at 370 K, and disappeared at 390 K. This profile clearly showed that the desorption proceeded through an intermediate with a highly regular crystal packing. This could be ascribed to the stepwise desorption of two equivalents of MeOH, although this might only be concluded unequivocally after structural determination of the intermediate.

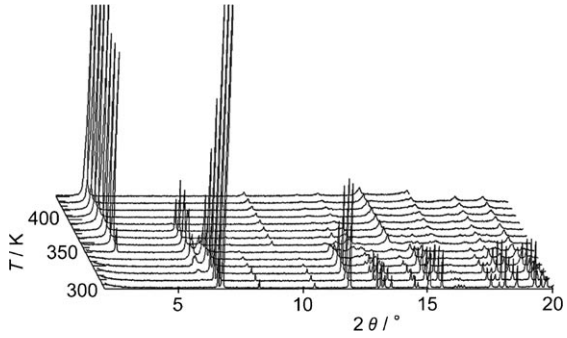

Figure 13. Temperature-dependent changes in synchrotron X-ray powder diffraction patterns of orange crystals **2**. Data were obtained at 10 K intervals from 300–430 K.

Vapor-dependent color change: Considering the structural changes of **1a** in **2** and **3** (Figure 9 and Figure 10), it was fairly certain that the observed color changes between **2** and **3** occurred through modulation of D–A interactions between PI and NDI units. This was verified by simulations of UV/Vis spectra by using DFT calculations (GGA/RPBE) based on the structural geometries determined by the synchrotron powder X-ray analysis. As shown in Figure 14, calculated spectra of a single molecular unit **1a** in both powders **2** and **3** had characteristic CT absorbances at 450–600 nm, the relative intensities of which were consistent with those of the experimental spectra (Figure 4).

The adsorption stoichiometry of other vapors such as EtOH, *i*PrOH, THF, and toluene strongly suggested that two equivalents of these guest molecules were included in a similar way to MeOH, although the adsorption efficiencies (1.4–1.7 equivalents) in most cases were slightly lower than for MeOH or EtOH (2.0 equivalents). Indeed, sharp XRD patterns were obtained from a strongly colored portion of solid **3** after exposure to various organic vapors, such as EtOH, *n*PrOH, *i*PrOH, 1-butanol, 2-butanol, *t*BuOH, Et_3N, DMSO, THF, and toluene (see the Supporting Information). This meant that the adsorption of these organic vapors also occurred by means of similar host–guest inclusion in the cavities of porous crystal **3** in a highly regular manner. Thus, the observed vapor-dependent color changes could again be attributed to these causes. In the adsorption of alcohol vapors, the D–A interaction peak at $\lambda = 450$–650 nm decreased in the order: MeOH > *n*PrOH > *i*PrOH > 2-BuOH > *t*BuOH, as shown in Figure 3. Thus, the color changes seen with alcohols could safely be attributed mainly to steric hindrance of intramolecular PI-NDI stacking interactions, as depicted in Scheme 1b,c. Adsorption of HCHO vapor resulted in a remarkable color change (red-purple to yellow) with high adsorption efficiency (6.3 equivalents). This was ascribed to similar, but strong interactions arising from its small molecular size and strong H-bonding ability. HCHO guest molecules might also have been included in many vacant sites around the PI and NDI moieties, leading to breakdown of the intramolecular PI-NDI interactions. This color change was consistent with the change from light-yellow to deep red seen upon melting of a 1:1 mixture of NDI and 1,5-dialkoxynaphthalene[11] for which a similar D–A interaction occurred after a crystalline-liquid phase transition.

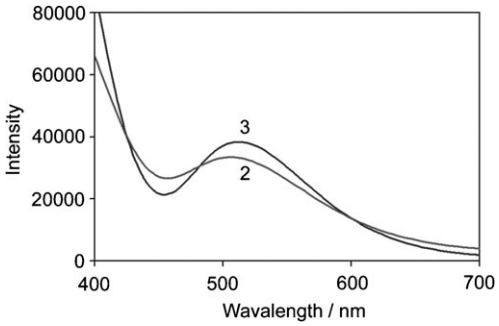

Figure 14. Simulated DFT (GGA/RPBE) UV/Vis spectra of **2** (recycled) and **3**.

It seemed reasonable to suppose that the color change to red-orange seen with non-H-bonding aromatic compounds arose mainly from stacking interactions with the aromatic planes of PINDI. Indeed, the various spectra of the powder containing adsorbed toluene showed different patterns from complexes incorporating the above H-bonding compounds. The CO stretching bands of the NDI moiety ($\nu_{as} = 1699$, $\nu_s = 1663\ cm^{-1}$) were typically shifted to lower frequency compared to crystals with MeOH (**2**, $\nu_s = 1702$, $\nu_{as} = 1664\ cm^{-1}$), THF ($\nu_s = 1705$, $\nu_{as} = 1667\ cm^{-1}$), Et_3N ($\nu_s = 1703$, $\nu_{as} = 1666\ cm^{-1}$) or to powder **3** ($\nu_s = 1705$, $\nu_{as} = 1665\ cm^{-1}$), which indicated that these carbonyl groups underwent weak H-bonding interactions exclusively upon exposure to toluene.

Furthermore, the broad CT absorbance was specifically enhanced in intensity in the $\lambda = 550$–650 nm region (Figure 4). These characteristic changes could be attributed to the formation of weak intermolecular H-bonds between NDI and neighboring PI units with slight modification of the intramolecular PI-NDI stacking mode. Presumably, planar aromatic guests partially stacked onto the extended NDI π-conjugated plane, inducing weak interference with intramolecular PI-NDI interactions. Consequently, slightly disordered NDI units could undergo weak intermolecular H-bonding with the pyrrole hydrogens of neighboring PI units to maintain packing stability. A schematic illustration of this structural change with planar aromatic compounds is shown in Scheme 1a.

Reversibility of adsorption: The strong adsorption capability of powder **3** could be attributed to the following two properties of PINDI crystals: 1) the ability of the S-shaped template to include a variety of H-bonding and non-H-bonding guest molecules; and 2) an interlocking mechanism preventing reversible dissociation of guest molecules, by switching of stacking stabilizations in crystal packing from intra- to intermolecular interactions. Scheme 2 shows a representation of the relation between adsorption properties and stacking interactions of these crystals. One equivalent of MeOH vapor was readily included in the cavities of these templates because of the facile permeation of MeOH molecules into the cavities through non-bonding gaps in **3**. The existence of the resulting intermediate **4** was strongly suggested both by the stepwise adsorption of MeOH (Figure 8) and the unidentified, sharp XRD pattern observed during the transformation of **2** to **3** (Figure 13). Inclusion of one guest molecule enhanced intermolecular PI-PI and NDI-NDI interactions, while weakening the intramolecular PI-NDI interaction. This slowed the adsorption of MeOH vapor as a result of the partial closing of the non-bonding gaps. Inclusion of a second equivalent of MeOH further strengthened the intermolecular interactions (Figure 11b), efficiently locking guest molecules in place, thus preventing their leakage. Stepwise desorption of MeOH, indicated by VT-XRD analysis (Figure 13), meant that dissociation of MeOH proceeded through the reverse pathway (two steps, sequentially breaking this interlocking mechanism).

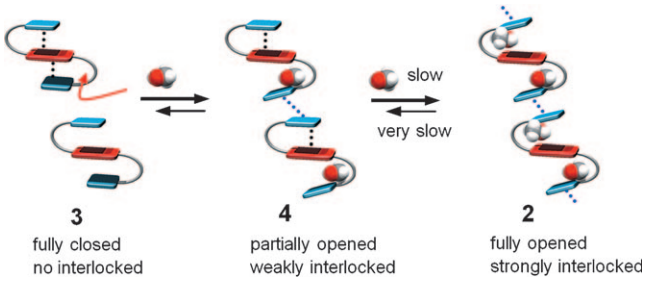

Scheme 2. Schematic representation of stepwise adsorption and desorption processes in PINDI crystals.

Reversible color changes were observed exclusively with MeOH, EtOH, and *n*PrOH. The solids that adsorbed other organic vapors did not regenerate red-purple solid **3** despite prolonged evacuation and/or heating. This irreversibility seen with most of the organic vapors adsorbed was not owed to disorder in the crystal packing, as their sharp XRD patterns (see the Supporting Information) indicated that they maintained their individual crystal packing structure. Rather, the packing structures of **2** and **3** (Figure 11) indicated that the reversibility of the color change could be attributed to the balance between intra- and intermolecular stabilizations. Thus, it was likely that these solids containing irreversibly adsorbed vapors incorporated strong, unbalanced intermolecular stabilizations, i.e., these structures contained tightly interlocked cavities, resulting in considerable degradation of PI-NDI stacking upon inclusion of vapor molecules.

Conclusion

In summary, we have synthesized the first vapochromic organic crystals (PINDI) showing unprecedented molecular-shape dependent color changes upon exposure to a variety of organic vapors. Various experimental results and structural investigations indicated that the cavities in, and flexible movement of, the S-shaped templates in PINDI crystals were crucial to their high adsorption capacity and vapochromic behavior. Flexible open–close motions of the S-shaped folding units in crystals were unequivocally established by synchrotron-radiation powder-diffraction experiments.

Experimental Section

General: *N*,*N*′-Bis(3-aminopropyl)-1,4,5,8-naphthalenetetracarboxylic diimide[15] and 4-*tert*-butylpyrrole-2-carboxaldehyde[16] were prepared according to the literature procedures. ^{1}H and ^{13}C NMR spectra were recorded by using a Varian Unity-Inova 500 spectrometer. IR spectra were obtained by using a Bruker Equinox 55 spectrometer. Optical micrograph images (Figure 1) were taken by using an Olympus BX41–31-D. SEM images (Figure 3) were obtained by using a Hitachi S-5000 L . UV/Vis spectra of solutions (Figure 6b) were recorded by using a Shimadzu MultiSpec-1500 spectrometer. Diffuse reflectance UV/Vis spectra of solids (Figure 4, 5, and 6a) were measured by using a Jasco V-570 spectrophotometer equipped with an integrated sphere using $BaSO_4$ as a matrix. Mass spectra were obtained by using a JEOL JMS-700 spectrometer. Elemental analysis was performed by using a Perkin–Elmer PE2400 microanalyzer. Thermogravimetric experiment (Figure 7) was carried out at a rate of 0.33°C min^{-1} under air atmosphere by using a Seiko Instrument TG/DTA 6200 analyzer. Adsorption/desorption isotherms (Figure 8) were measured by using a Bel Belsorp 18 plus volumetric adsorption analyzer.

***N*,*N*′-Bis{3-[(4-*tert*-butylpyrrol-2-ylmethylene)amino]propyl}-1,4,5,8-naphthalenetetracarboxylic diimide (1a)**: A mixture of *N*,*N*′-Bis(3-aminopropyl)-1,4,5,8-naphthalenetetracarboxylic diimide (0.471 g, 0.772 mmol), 4-*tert*-butylpyrrole-2-carboxaldehyde (0.289 g, 1.91 mmol), and Na_2CO_3 (0.102 g, 1.04 mmol) in MeOH (20 mL) was stirred for 14 h at room temperature. The resulting orange precipitate was collected, washed successively with water and hexane, and dried in vacuo to give **1a** (0.463 g, 93%) as a red-purple powder. ^{1}H NMR (500 MHz, $CDCl_3$): $\delta = 1.20$ (s,

18H; C(CH_3)$_3$), 2.14 (tt, J=7.0, 7.0 Hz, 4H; $CH_2CH_2CH_2$), 3.63 (t, J=7.0 Hz, 4H; CH=NCH_2), 4.31 (t, J=7.0 Hz, 4H; CH_2NCO), 6.29 (d, J=1.5 Hz, 2H; H^3 in pyrrole), 6.49 (d, J=1.5 Hz, 2H; H^5 in pyrrole), 7.98 (s, 2H; CH=N), 8.69 ppm (s, 4H; H^2, H^3, H^6, H^7 in NDI); ^{13}C NMR (126 MHz, $CDCl_3$): δ=162.9, 152.2, 136.8, 130.8, 129.4, 126.5, 126.4, 117.3, 112.3, 58.4, 39.3, 31.6, 30.4, 29.0; UV/Vis (toluene) λ_{max}(log ε)=294 (4.63), 363 (4.28), 382 nm (4.31 mol^{-1}dm^{3}cm^{-1}); FABMS: m/z: 647.8 (M+H)$^+$; HRMS calcd for $C_{38}H_{43}N_6O_4$: 647.3346; found: 647.3346.

Preparation of crystal 2 (1a·2MeOH): Recrystallization of **1a** from MeOH and DMSO gave **2** as orange needles. IR (KBr): $\tilde{\nu}$=1702 (CO), 1664 (CO), 1639 cm^{-1} (C=N); UV/Vis ($BaSO_4$): λ_{max}=300, 366, 383, 511 nm; elemental analysis (%) calcd for $C_{40}H_{50}O_6N_6$: C 67.58, H 7.09, N 11.82; found: C 67.84, H 7.34, N 11.82.

Preparation of adsorbent powder 3 (1a): Crystals **2** (102 mg, 0.143 mmol) were finely ground into a micropowder, and dried in vacuo at 353 K to give **3** (92.9 mg, 100%) as a red purple powder. IR (KBr): $\tilde{\nu}$=1705 (CO), 1665 (CO), 1636 cm^{-1} (C=N); UV/Vis ($BaSO_4$): λ_{max}=304, 362, 378, 534 nm; elemental analysis (%) calcd for $C_{38}H_{42}O_4N_6$: C 70.57, H 6.55, N 12.99; found: C 70.42, H 6.48, N 12.87.

Color change of powder 3 upon exposure to organic vapors: A 2 mL flat-bottomed glass cell charged with powder **3** (2 mg), was placed in a 50 mL wide-mouth flat-bottomed glass bottle with a seal cap. Organic solvent (2 mL) was poured into the wide-mouth bottle without direct contact with **3**. The vessel was capped and allowed to stand at room temperature. Color changes of **3** were observed visually, or spectroscopically by diffuse reflectance UV/Vis analysis. 30% Aqueous solution of HCHO (formalin) was used for exposure to HCHO vapor. Exposure to MeOH, EtOH, *i*PrOH, THF, HCHO, and toluene vapors resulted in weight gains of 9.8, 14, 13, 19, 29, and 14%, corresponding to the inclusion of 2.0, 2.0, 1.4, 1.7, 6.3, and 1.5 equivalents of the guest molecules, respectively. Color change experiments under low concentration of organic vapors were carried out similarly in a 500 mL glass vacuum desiccator.

X-ray structure determination:

Single crystal X-ray diffraction: Orange-red crystals **2** suitable for X-ray diffraction studies were analyzed by using a Rigaku R-AXIS RAPID imaging plate diffractometer with graphite-monochromated $Mo_{K\alpha}$ radiation (λ=0.71075 Å) (Table 1, Figure 9). The structure of **2** was solved by direct methods and refined by the full-matrix least-squares method. In the subsequent refinement, the function $\Sigma\omega(F_o^2-F_c^2)^2$ was minimized for which (F_o) and (F_c) were the observed and calculated structure factor amplitudes, respectively. The positions of all non-hydrogen atoms were found from difference Fourier electron density maps and refined anisotropically. All calculations were performed using the teXsan crystallographic software package.

Powder X-ray diffraction: Red-purple powder **3** suitable for powder X-ray diffraction was prepared according to the following procedure. Crude solid **3**, prepared as above, was dissolved completely in hot toluene. Precipitation upon rapid cooling gave a mixture of **3** and an unidentified orange-red toluene complex. Analytical grade, red-purple microcrystals **3** could be separated manually because of their distinct color. Regenerated orange sample **2** for structure determination was prepared by exposure of crude **3** to MeOH vapor according to the above procedure for color change. The X-ray powder diffraction patterns of **3** and **2** (recycled) were measured with $Cu_{K\alpha}$ radiation (λ=1.5418 Å) by using a Philips X'Pert-MPD diffractometer (Figure 12) and synchrotron radiation (λ=1.30 Å) using imaging plate detectors and the large Debye–Scherrer camera on the BL19B2 beamline at the Super Photon Ring (SPring-8, Hyogo, Japan) (Table 1, Figure 10, 11, and 13). The diffraction patterns were indexed by using DICVOL91[19] to obtain lattice parameters that were subsequently refined in a Pawley fit.[20] Z-Matrices describing the molecular topology of the fragments in the compound were generated automatically by DASH[17] from the structural data of crystal **2**. Twenty five runs with 10^7 simulated annealing (SA) moves per run were performed for structure solution. A final Rietveld refinement was performed by using the RIETAN-FP[18] program. CCDC-747785 (**2**), CCDC-747787 (powder **3**), CCDC 747786 (recycled powder **2**) contains the supplementary crystallographic data for this paper. These data can be obtained free of charge from The Cambridge Crystallographic Data Centre via www.ccdc.cam.ac.uk/data_request/cif.

Computational methods: For satisfactory simulation of the UV/Vis spectra, geometries of **2** and **3** were optimized based on the initial data from Rietveld refinement. All calculations were carried out using first-principles plane-wave functional theory as implemented in the CASTEP[21] code of the Materials Studio (MS) package. For the exchange and correlation terms, the generalized gradient approximation (GGA) was used in the revised Perdew, Burke, Ernzerhof (GGA-PBE) scheme[22] with ultrasoft pseudopotentials.[23] The electronic wave functions were expanded in a plane wave basis set with a 300 eV energy cut-off. Pseudo-atomic calculations were performed for H $1s^1$, C $2s^22p^2$, N $2s^22p^3$, and O $2s^22p^4$. For the Brillouin-zone sampling 3×3×2 Monkhorst-Pack[24] meshes were used for the structures of **2** and **3**, where the self-consistent convergence of the total energy was 2.0×10^{-6} eV/atom. The calculations were performed except for cell parameters using BFGS[25] and damped molecular dynamics. After structural deviations found by this optimization process were confirmed to be sufficiently negligible for qualitative discussion (see Supporting Information), the data were used to calculate electronic band structures and density of states (DOS), and subsequent simulation of UV/Vis spectra was performed using the program bundled with the MS package.

Acknowledgements

This work was supported by a Grant-in-Aid for Scientific Research, from the Ministry of Education, Culture, Sports, Science and Technology, Japan, and PRESTO of Japan Science and Technology (JST). We thank Dr. D. Hashizume (RIKEN), Dr. K. Miura (JASRI), Dr. F. Izumi (NIMS), and Prof. Y. Ohashi (JASRI) for powder X-ray analysis. E.T. express his special thanks to the Global COE program "Global Education and Research Center for Bio-Environmental Chemistry" for financial support.

[1] R. Matsushima, N. Nishimura, K. Goto, Y. Kohno, *Bull. Chem. Soc. Jpn.* **2003**, *76*, 1279–1283.
[2] A. B. Descalzo, M. D. Marcos, C. Monte, R. Martínez-Máñez, K. Rurack, *J. Mater. Chem.* **2007**, *17*, 4716–4723.
[3] D. Li, C. A. Mills, J. M. Cooper, *Sens. Actuators B* **2003**, *92*, 73–80.
[4] Pt: a) C. L. Exstrom, J. R. Sowa, Jr., C. A. Daws, D. Janzen, K. R. Mann, G. A. Moore, F. F. Stewart, *Chem. Mater.* **1995**, *7*, 15–17; b) C. A. Daws, C. L. Exstrom, J. R. Sowa, Jr., K. R. Mann, *Chem. Mater.* **1997**, *9*, 363–368; c) C. E. Buss, C. E. Anderson, M. K. Pomije, C. M. Lutz, D. Britton, K. R. Mann, *J. Am. Chem. Soc.* **1998**, *120*, 7783–7790; d) Y. Kunugi, K. R. Mann, L. L. Miller, C. L. Exstrom, *J. Am. Chem. Soc.* **1998**, *120*, 589–590; e) Y. Kunugi, L. L. Miller, K. R. Mann, M. K. Pomije, *Chem. Mater.* **1998**, *10*, 1487–1489; f) Reference [2b]; g) C. E. Buss, K. R. Mann, *J. Am. Chem. Soc.* **2002**, *124*, 1031–1039; h) M. Kato, A. Omura, A. Toshikawa, S. Kishi, Y. Sugimoto, *Angew. Chem.* **2002**, *114*, 3315–3317; *Angew. Chem. Int. Ed.* **2002**, *41*, 3183–3185; i) L. J. Grove, J. M. Rennekamp, H. Jude, W. B. Connick, *J. Am. Chem. Soc.* **2004**, *126*, 1594–1595; j) T. J. Wadas, Q.-M. Wang, Y.-J. Kim, C. Flaschenreim, T. N. Blanton, R. Eisenberg, *J. Am. Chem. Soc.* **2004**, *126*, 16841–16849; k) M. Kato, S. Kishi, Y. Wakamatsu, Y. Sugi, Y. Osamura, T. Koshiyama, M. Hasegawa, *Chem. Lett.* **2005**, *34*, 1368–1369; l) P. Du, J. Schneider, W. W. Brennessel, R. Eisenberg, *Inorg. Chem.* **2008**, *47*, 69–77; m) L. J. Grove, A. G. Oliver, J. A. Krause, W. B. Connick, *Inorg. Chem.* **2008**, *47*, 1408–1410.
[5] Au a) M. A. Mansour, W. B. Connick, R. J. Lachicotte, H. J. Gysling, R. Eisenberg, *J. Am. Chem. Soc.* **1998**, *120*, 1329–1330; b) M. A. Rawashdeh-Omary, M. A. Omary, J. P. Fackler, Jr., R. Galassi, B. R. Pietroni, A. Burini, *J. Am. Chem. Soc.* **2001**, *123*, 9689–9691; c) E. J. Fernández, J. M. López-de-Luzuriaga, M. Monge, M. E. Olmos, J. Pérez, A. Laguna, A. A. Mohamed, J. P. Fackler, Jr., *J. Am. Chem.*

Soc. **2003**, *125*, 2022–2023; d) E. J. Fernández, J. M. López-de-Luzuriaga, M. Monge, M. Montiel, M. E. Olmos, J. Pérez, A. Laguna, F. Mendizabal, A. A. Mohamed, J. P. Fackler, Jr., *Inorg. Chem.* **2004**, *43*, 3573–3581; e) J. Lefebvre, R. J. Batchelor, D. B. Leznoff, *J. Am. Chem. Soc.* **2004**, *126*, 16117–16125.

[6] a) Co: L. G. Beauvais, M. P. Shores, J. R. Long, *J. Am. Chem. Soc.* **2000**, *122*, 2763–2772; b) Ag: E. J. Fernández, J. M. López-de-Luzuriaga, M. Monge, M. E. Olmos, R. C. Puelles, A. Laguna, A. A. Mohamed, J. P. Fackler, Jr., *Inorg. Chem.* **2008**, *47*, 8069–8076.

[7] Cu a) K. Yamada, S. Yagishita, H. Tanaka, K. Tohyama, K. Adachi, S. Kaizaki, H. Kumagai, K. Inoue, R. Kitaura, H.-C. Chang, S. Kitagawa, S. Kawata, *Chem. Eur. J.* **2004**, *10*, 2647–2660; b) K. Yamada, H. Tanaka, S. Yagishita, K. Adachi, T. Uemura, S. Kitagawa, S. Kawata, *Inorg. Chem.* **2006**, *45*, 4322–4324.

[8] Pt a) W. Lu, M. C. W. Chan, K.-K. Cheung, C.-M. Che, *Organometallics* **2001**, *20*, 2477–2486; b) W. Lu, M. C. W. Chan, N. Zhu, C.-M. Che, Z. He, K.-Y. Wong, *Chem. Eur. J.* **2003**, *9*, 6155–6166; Ir c) Z. Liu, Z. Bian, J. Bian, Z. Li, D. Nie, C. Huang, *Inorg. Chem.* **2008**, *47*, 8025–8030; Ru d) K. A. McGee, B. J. Marquardt, K. R. Mann, *Inorg. Chem.* **2008**, *47*, 9143–9145.

[9] a) K. C. Gupta, A. G. Ulsamer, P. W. Preuss, *Environ. Int.* **1982**, *8*, 349–358; b) *Formaldehyde: Analytical Chemistry and Technology* (Ed.: V. Turoski), ACS, Washington, **1985**.

[10] a) M. S. Cubberley, B. L. Iverson, *J. Am. Chem. Soc.* **2001**, *123*, 7560–7563; b) X.-Z. Wang, X.-Q. Li, X.-B. Shao, X. Zhao, P. Deng, X.-K. Jiang, Z.-T. Li, Y.-Q. Chen, *Chem. Eur. J.* **2003**, *9*, 2904–2913; c) S. A. Vignon, T. Jarrosson, T. Iijima, H.-R. Tseng, J. K. M. Sanders, J. F. Stoddart, *J. Am. Chem. Soc.* **2004**, *126*, 9884–9885; d) T. Iijima, S. A. Vignon, H.-R. Tseng, T. Jarrosson, J. K. M. Sanders, F. Marchioni, M. Venturi, E. Apostoli, V. Balzani, J. F. Stoddart, *Chem. Eur. J.* **2004**, *10*, 6375–6392; e) G. D. Pantoş, P. Pengo, J. K. M. Sanders, *Angew. Chem.* **2007**, *119*, 198–201; *Angew. Chem. Int. Ed.* **2007**, *46*, 194–197; f) G. Koshkakaryan, K. Parimal, J. He, X. Zhang, Z. Abliz, A. H. Flood, Y. Liu, *Chem. Eur. J.* **2008**, *14*, 10211–10218.

[11] J. J. Reczek, K. R. Villazor, V. Lynch, T. M. Swager, B. L. Iverson, *J. Am. Chem. Soc.* **2006**, *128*, 7995–8002.

[12] A comprehensive review of foldamers: D. J. Hill, M. J. Mio, R. B. Prince, T. S. Hughes, J. S. Moore, *Chem. Rev.* **2001**, *101*, 3893–4011.

[13] a) R. S. Lokey, B. L. Iverson, *Nature* **1995**, *375*, 303–305; b) J. Q. Nguyen, B. L. Iverson, *J. Am. Chem. Soc.* **1999**, *121*, 2639–2640; c) A. J. Zych, B. L. Iverson, *J. Am. Chem. Soc.* **2000**, *122*, 8898–8909; d) G. J. Gabriel, B. L. Iverson, *J. Am. Chem. Soc.* **2002**, *124*, 15174–15175; e) G. J. Gabriel, S. Sorey, B. L. Iverson, *J. Am. Chem. Soc.* **2005**, *127*, 2637–2640.

[14] a) N. Yoshida, T. Ishizuka, K. Yofu, M. Murakami, H. Miyasaka, T. Okada, Y. Nagata, A. Itaya, H. S. Cho, D. Kim, A. Osuka, *Chem. Eur. J.* **2003**, *9*, 2854–2866; b) M. Borgström, N. Shaikh, O. Johansson, M. F. Anderlund, S. Styring, B. Åkermark, A. Magnuson, L. Hammarström, *J. Am. Chem. Soc.* **2005**, *127*, 17504–17515.

[15] M. Licchelli, L. Linati, A. O. Biroli, E. Perani, A. Poggi, D. Sacchi, *Chem. Eur. J.* **2002**, *8*, 5161–5169.

[16] R. M. Silverstein, E. E. Ryskiewicz, C. Willard, *Org. Synth. Coll. Vol. 4*, **1963**, 831–833.

[17] DASH (3.01), W. I. F. David, K. Shankland, Cambridge Crystallographic Data Centre, Cambridge, **2004**.

[18] a) F. Izumi, T. Ikeda, *Mater. Sci. Forum* **2000**, *198*, 321–324; b) F. Izumi, K. Momma, *Solid State Phenom.* **2007**, *130*, 15–20.

[19] A. Boultif, D. Louër, *J. Appl. Crystallogr.* **1991**, *24*, 987–993.

[20] G. S. Pawley, *J. Appl. Crystallogr.* **1981**, *14*, 357–361.

[21] S. J. Clark, M. D. Segall, C. J. Pickard, P. J. Hasnip, M. J. Probert, K. Refson, M. C. Payne, *Z. Kristallogr.* **2005**, *220*, 567–570.

[22] J. P. Perdew, K. Burke, M. Ernzerhof, *Phys. Rev. Lett.* **1996**, *77*, 3865–3868.

[23] K. Laasonen, A. Pasquarello, R. Car, C. Lee, D. Vanderbilt, *Phys. Rev. B* **1993**, *47*, 10142–10153.

[24] H. J. Monkhorst, J. D. Pack, *Phys. Rev. B* **1976**, *13*, 5188–5192.

[25] B. G. Pfrommer, M. Cote, S. G. Louie, M. L. Cohen, *J. Comput. Phys.* **1997**, *131*, 233–240.

Received: December 11, 2009
Published online: March 15, 2010

